RESEARCH ARTICLE

JOR *Spine* OPEN ACCESS

Clinical implications of linking microstructure, spatial biochemical, spatial biomechanical, and radiological features in ligamentum flavum degeneration

Azril Azril[1] | Kuo-Yuan Huang[2] | Hsin-Yi Liu[1] | Wei-An Liao[3] |
Wen-Lung Liu[2] | Jonathan Hobley[1] | Yeau-Ren Jeng[1,4,5]

[1]Department of Biomedical Engineering, National Cheng Kung University, Tainan City, Taiwan

[2]Department of Orthopedics, National Cheng Kung University Hospital, College of Medicine, Tainan City, Taiwan

[3]Department of Pathology, National Cheng Kung University Hospital, College of Medicine, National Cheng Kung University, Tainan City, Taiwan

[4]Academy of Innovative Semiconductor and Sustainable Manufacturing, National Cheng Kung University, Tainan City, Taiwan

[5]Medical Device Innovation Center, National Cheng Kung University, Tainan City, Taiwan

Correspondence
Yeau-Ren Jeng, Department of Biomedical Engineering, National Cheng Kung University, Tainan City, Taiwan.
Email: imeyrj@gs.ncku.edu.tw

Abstract

Background: The ligamentum flavum (LF) degeneration is a critical factor in spinal stenosis, leading to nerve compression and pain. Even with new treatment options becoming available, it is vital to have a better understanding of LF degeneration to ensure the effectiveness of these treatments.

Objective: This study aimed to provide insight into LF degeneration by examining the connections between various aspects of LF degeneration, including histology, microstructure, chemical composition, and biomechanics.

Method: We analyzed 30 LF samples from 27 patients with lumbar vertebrae, employing magnetic resonance imaging (MRI) to link lumbar disc degeneration grades with fibrosis levels in the tissue. X-ray diffraction (XRD) analysis assessed microstructural alterations in the LF matrix component due to degeneration progression. Instrumented nanoindentation combined with Raman spectroscopy explored the spatial microbiomechanical and biochemical characteristics of the LF's ventral and dorsal regions.

Results: Our outcomes revealed a clear association between the severity of LF fibrosis grades and increasing LF thickness. XRD analysis showed a rise in crystalline components and hydroxyapatite molecules with progressing degeneration. Raman spectroscopy detected changes in the ratio of phosphate, proteoglycan, and proline/hydroxyproline over the amide I band, indicating alterations in the extracellular matrix

---

Azril Azril and Kuo-Yuan Huang authors are contribute equally.

composition. Biomechanical testing demonstrated that LF tissue becomes stiffer and less extensible with increasing fibrosis.

Discussion: Notably, the micro-spatial assessment revealed the dorsal side of the LF experiencing more significant mechanical stress, alongside more pronounced biochemical and biomechanical changes compared to the ventral side. Degeneration of the LF involves complex processes that affect tissue histology, chemical composition, and biomechanics. It is crucial to fully understand these changes to develop new and effective treatments for spinal stenosis. These findings can improve diagnostic accuracy, identify potential biomarkers and treatment targets, guide personalized treatment strategies, advance tissue engineering approaches, help make informed clinical decisions, and educate patients about LF degeneration.

KEYWORDS
biomechanics, ligamentum flavum, microstructure, nanoindentation, radiology assessment, Raman spectroscopy

1 | INTRODUCTION

Pathological changes in the ligamentum flavum (LF) cause it to lose strength and elasticity, resulting in function restriction and contraction of the nervous tissue in the vertebral canal and back pain.[1] These changes are often linked to LF hypertrophy (LFH), characterized by tissue thickening, enlargement, and fibrosis, contributing to LF degeneration.[2]

Management of LFH hinges on symptom severity and the extent of the spinal cord or nerve compression. Initial treatments encompass conservative approaches such as physical therapy, pain management, and activity modification.[3] Surgical intervention is considered for refractory symptoms or severe conditions involving decompressive procedures targeting the spinal canal.[4] Emerging research explores novel LFH treatments like decorin therapy[5] and oxidative stress therapy.[6] However, an in-depth investigation is necessary to establish treatment efficacy, mainly by focusing on spatial LF characteristics.

Various studies have investigated LF degeneration, including age-related stiffness elevation under tensile stress and calcification.[7] Prior assessments often overlooked the heterogeneous nature of biological tissue, relying primarily on qualitative analyses. Recognizing the importance of spatial attributes, this study aims to comprehensively evaluate fiber characteristics, radiographic features (MRI), microstructure, micro-spatial biomechanics, and the chemical composition of LF in patients with degenerative disc disease.

To achieve micro-spatial biomechanical and chemical evaluations, this study employs instrumented nanoindentation concurrently with Raman spectroscopy, building upon our previous research endeavors.[8–10] Nanoindentation, a well-established method for characterizing the mechanical properties of biological tissues, offers advantages over Atomic Force Microscopy (AFM) by automating numerous measurements across substantial areas via depth-sensing techniques[11] and precision positioning stage and scanning systems that can localize the sample characteristics.[12] The nanoscale Dynamic

Mechanical Analysis (NanoDMA) mode of indentation used in this study effectively assesses tissue viscoelasticity during dynamic testing.

Raman spectroscopy, recognized for probing the chemical composition and intermolecular interactions in biological samples, is a valuable tool for identifying specific spectral signatures associated with tissue diseases like skin evaluation[13] and cartilage assessment.[14] Unlike complex histology techniques, Raman spectroscopy necessitates minimal sample preparation and provides insight into tissue component chemical structures. The clinical application of Raman spectroscopy enhances the understanding of tissue heterogeneity.[15]

This study emphasizes the micro-spatial exploration of LF, which still needs to be extensively studied. Our approach unveils the LF's heterogeneity in biochemical and biomechanical attributes, requiring a minimal sample size for characterization. The correlative analysis of LF features with degenerative changes offers valuable insights, bolstering diagnostic precision, pathological comprehension, treatment development, monitoring strategies, outcome assessment, and technological advancements.

2 | MATERIALS AND METHODS

2.1 | Patient samples retrieval and preservation

This study involved 27 participants (10 men and 17 women) with the diagnosis of lower lumbar (L3-5) or lumbosacral (L5-S1) degeneration who suffered from low back pain, sciatica or claudication and unresponsive to conservative treatments more than 6 months were included in the study. These surgeries were explicitly aimed at addressing spinal degeneration issues like spinal stenosis (including central, lateral recess, or foraminal stenosis), degenerative spondylolisthesis, or degenerative scoliosis. Individuals with spinal conditions stemming from infections or tumors were excluded. All the enrolled patients

underwent posterior spinal decompressive procedures, such as laminotomy, partial or total laminectomy with or without posterolateral spinal fusion, and posterior or transforaminal interbody fusion if vertebral intersegmental instability was detected. Ethical clearance for the study was granted by the NCKUH Review Board (NCKUH-IRB no. B-BR-109-068). A total of 30 LF samples were retrieved from different lumbar or lumbosacral locations. Following harvest, the LF tissues were placed in sterile plastic containers and transported on ice to the laboratory for further processing. The tissues were thoroughly rinsed with phosphate-buffered saline (PBS) until the wash solution exhibited minimal blood coloration. Subsequently, fixation was performed using 4% paraformaldehyde (PFA), as previously described in.[16] To briefly explain the sample preparation process, the samples were embedded in paraffin, affixed to quartz slide substrates, and then hydrated using a PBS solution. Only tissues with clearly identifiable ventral and dorsal regions were included in this study.

2.2 | Fibrosis classification and fiber orientation of patient samples

Fibrosis severity in patient samples was determined using hematoxylin and eosin (H&E) staining and a multi-criteria approach considering morphology, radiological features, biochemical properties, and biomechanical characteristics. Three distinct grades were defined: Grade 1, with well-organized parallel elastic fibers; Grade 2, with a mixture of wavy elastic and collagen fibers; and Grade 3, characterized by significantly disorganized or hyalinized collagen fibers. Fiber orientation was then quantified using ImageJ's Directionality plugin. Following a specific workflow, color images were converted to grayscale; then, fibers were enhanced with the Tubeness plugin. The Directionality plugin subsequently measured fiber alignment and generated orientation data (fiber dispersion), which was visualized and quantified as a histogram of fiber distribution across the range of 0 to 180 degrees. The fiber dispersions of each sample grade were plotted. A low dispersion value means the fibers are tightly aligned around the dominant direction. A high dispersion value suggests the fibers are more randomly oriented, lacking a robust directional preference.

2.3 | Radiological evaluation of patients

The patient evaluation included a comprehensive analysis of lumbar MRI scans to assess factors potentially associated with LF degeneration: LF thickness, intervertebral disc (IVD) health, and foraminal dimensions. LF thickness was meticulously measured using the Dicom Works software, ensuring accuracy and consistency. Disc health was evaluated using the Pfirrmann grading system, which comprehensively considers IVD structure, signal intensity, nucleus pulposus and annulus fibrosus differentiation, and disc height.[17] This multi-faceted approach provided a detailed picture of the potential contributors to LF thickening and spinal canal stenosis

2.4 | Phase analysis of LF microstructure

LF phase changes due to degeneration were analyzed using X-ray diffraction (XRD) with a two-dimensional X-ray diffractometer: D8 Discover with GADDS (Bruker AXS Gmbh, Karlsruhe, Germany). Before the testing, the samples were detached from the substrate. Four samples from each fibrosis grade were ground together and put on the silicon wafer substrate to reduce the noise of the XRD signals. The 2θ scanning range was from 5 to 60°. The measurement conditions were as follows, CuK-α radiation: 1.54184 Å (0.154184 nm), Power: 40 kV and 40 mA; Beam size: 1.0 mm (the collimator system allows the analysis of 1000 μm^2 surface areas); detector type: Vantec-2000 (14×14 cm^2 area and 2048×2048-pixel density); Sample to detector distance: 15.03 cm; exposure time: 300 s/frame.

2.5 | Biochemical content assessment in Raman spectroscopy

Raman spectroscopy was used to determine the chemical composition of the LF samples, and the specifics of this system have been described previously in.[10,18] The relative intensity of Raman peaks was used to determine the compositional changes. This study focused on the Proline/Hydroxyproline changes (strong peak at 851 cm^{-1}), mineral changes (peak at 958 cm^{-1}), and proteoglycan (1064 and 1370 cm^{-1}) shifts toward the amide I (peak at 1656 cm^{-1}) as the main component of extracellular matrix (ECM). The mineralization was determined by comparing the relative concentration of mineral phosphate (peak at 958 cm^{-1}) to the intensity of amide I, the principal component of ECM (peak at 1656 cm^{-1}).[19]

The following are the parameters for the Raman measurement: the probe laser power was 4.3 mW at a wavelength of 532 nm; the microscope objective has a magnification of 100×, a working distance of 0.35 mm, a numerical aperture of 0.5, a spectral range of 800–1700 cm^{-1}, and the grating: 1800 lines/mm. The exposure time for each point was 10 s, and there were 225 sample points on each side (dorsal/ventral). The collection parameters were optimized to protect the sample from any potential photothermal damage caused by probe laser exposure. Each scan used a different position (operating mapping mode). The average of the Raman maps was used to assess the average spectra and, consequently, the chemical composition of the tissue.

2.6 | Biomechanical evaluation

The biomechanical properties of LF samples were assessed using a NanoDMA III Hysitron Triboindenter TI 980. Quasi-static and dynamic analyses were conducted to determine reduced modulus, hardness, storage modulus, and loss modulus. NanoDMA measurements were performed with specific parameters, and an optical microscope aided the indentation process. Sample indentation points ranged from 100 to 150.

TABLE 1 Parameter of NanoDMA for biomechanical assessment.

Parameter	Data
Indenter tip	Berkovich diamond tip with a radius of ~150 nm
Load-controlled algorithm	Linear CMX
Preload (P_o)	1 μN
Constant force (P_{max})	80 μN
Frequency	50 Hz
Quasi-static dwell time	5 s

TABLE 2 Cohen's guidelines for interpreting the results of the correlation coefficient.

Interpretation	Correlation value, rs (positive or negative)
Small correlation	0 to 0.29
Medium correlation	0.3 to 0.4
Large correlation	0.5 to 1

NanoDMA was executed using the CMX-mode (Linear Continuous Measurement of X) with the parameters shown in Table 1. This type of test will perform continuous measurements of X (various parameters such as reduced modulus, hardness, etc.). To assist with the dorsal and ventral sides of the LF samples, an optical microscope (IEEE 1394 CCD camera) was utilized with 0.5× digital camera magnification, 20× fixed optical magnification, 10× total magnification, 626 m horizontal size, and 552 m vertical size.

2.7 | Statistical analysis

The data were analyzed using OriginPro 2024. One-way analysis of variance (ANOVA) and Tukey's test for multiple comparisons determined significant differences among groups. Spearman's rank correlation coefficient (ρ) was acquired to determine the correlation among the variables of LF fibrosis grading. Spearman's rank correlation coefficient (ρ) was used to assess the strength and direction of the associations between these variables. The interpretation of the level of correlation coefficient of the research follows the guidelines given by Cohen,[20] where the correlation values, represented by rs, depend on the magnitude and can be categorized as small, medium, or large correlation, as shown in Table 2. Statistical significance was defined at $p = 0.05$.

3 | RESULTS

3.1 | Classification of fibrosis grading and fiber orientation

The distribution of fibrosis severity across patient samples is presented in Figure 1 (A). A total of 30 samples were collected from 27 patients, demonstrating a repartition of fibrosis grades: grade 1 ($n = 9$), grade 2 ($n = 15$), and grade 3 ($n = 6$). Figure 1(B) illustrates the fiber dispersion for each grade in the ventral and dorsal regions. Grade 1 fibrosis demonstrates the lowest dispersion, indicating tightly aligned collagen/elastin fibers around a dominant direction. As severity increases, fiber dispersion also increases, signifying a more random orientation. All grades show statistically significant differences in fiber dispersion ($p < 0.05$). Representative fiber visualizations are shown in Figure 1(C)–(K). The H&E staining further elucidates the morphological changes associated with fibrosis progression. Grade 1 exhibits a well-organized, parallel fiber arrangement, while grade 2 displays disrupted fiber alignment. At advanced fibrosis (grade 3), significant disorganization and hyalinized collagen deposition are observed. Grade 1 tissue demonstrates a highly parallel fiber orientation tightly aligned around the dominant direction. In contrast, grade 2 exhibits a more random, randomly oriented fiber distribution, lacking a strong directional preference with fiber dispersion. This trend continues in grade 3, which shows the most substantial disorientation with fiber dispersion. The corresponding fiber alignment histograms further confirm the significantly higher parallelism of fibers in grade 1 compared to the other grades.

3.2 | Evaluation of patient samples by radiology

Figure 2(A,B) illustrate the relationship between LF thickness and fibrosis grades. Interestingly, while the average thickness increases across grades (3.4 ± 0.5 mm for grade 1, 4.0 ± 0.10 mm for grade 2, and 6.1 ± 1.4 mm for grade 3), statistically significant differences emerge only between grade 2 and grade 3 ($p < 0.05$). Despite no significant difference between grades 1 and 2 ($p = 0.45$), the overall trend implies a correlation between fibrosis severity and LF thickening ($p < 0.05$).

Figure 2(C) displays representative sagittal MRI images demonstrating the Pfirrmann grading system for IVD degeneration. Notably, fibrosis was observed in samples corresponding to Pfirrmann grades II to V, suggesting a potential link between disc degeneration and collagen architecture changes within the LF. Figure 2(D) further reinforces this connection. It showcases the distribution of fibrosis samples across different Pfirrmann grades, revealing that while mild degeneration (Pfirrmann grade II) can exhibit fibrosis, most affected samples fall within grades III, IV, and V.

3.3 | Phase analysis

The XRD patterns of the LF tissue revealed changes in crystallinity and mineral composition associated with increasing fibrosis grades Figure 3(A). The characteristic peaks of collagen/elastin in the XRD pattern are reported to be a weak diffraction peak at ~8° and a broad hump at ~22°, indicating that the collagen sample has a low crystallinity.[21] The other broad and weak peak at ~43° also matches well with the reported XRD spectra for collagen[21,22] And can be found in grades
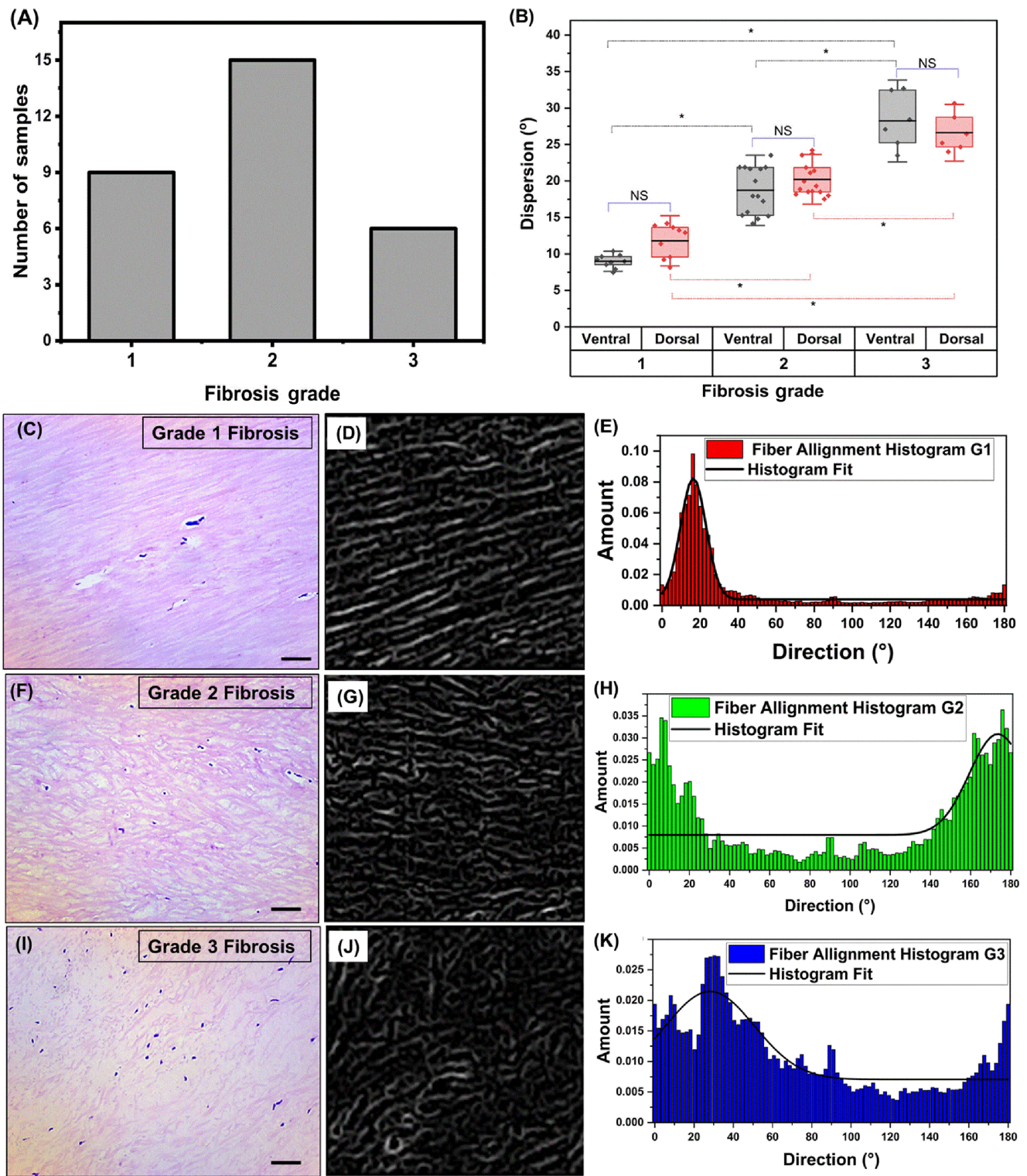
FIGURE 1   (A) Thirty samples with varying fibrosis grades were obtained from 27 patients. (B) Statistical analysis of fiber alignment determined by the fiber dispersion. (C–E) Representative grades 1 fibrosis: H&E staining of tissue, black and white fiber orientation, and fiber alignment histogram, respectively. (F–H) Representative grades 2 fibrosis: H&E staining of tissue, black and white fiber orientation, and fiber alignment histogram, respectively. (I–K) Representative grades 3 fibrosis: H&E staining of tissue, black and white fiber orientation, and fiber alignment histogram, respectively. All representatives of H&E staining of tissues, black and white fiber orientation, and fiber alignment histogram were taken from the dorsal side of each grade. The black scale bar on H&E staining images represents 50 μm. NS, Not statistically different, *: $p < 0.05$.
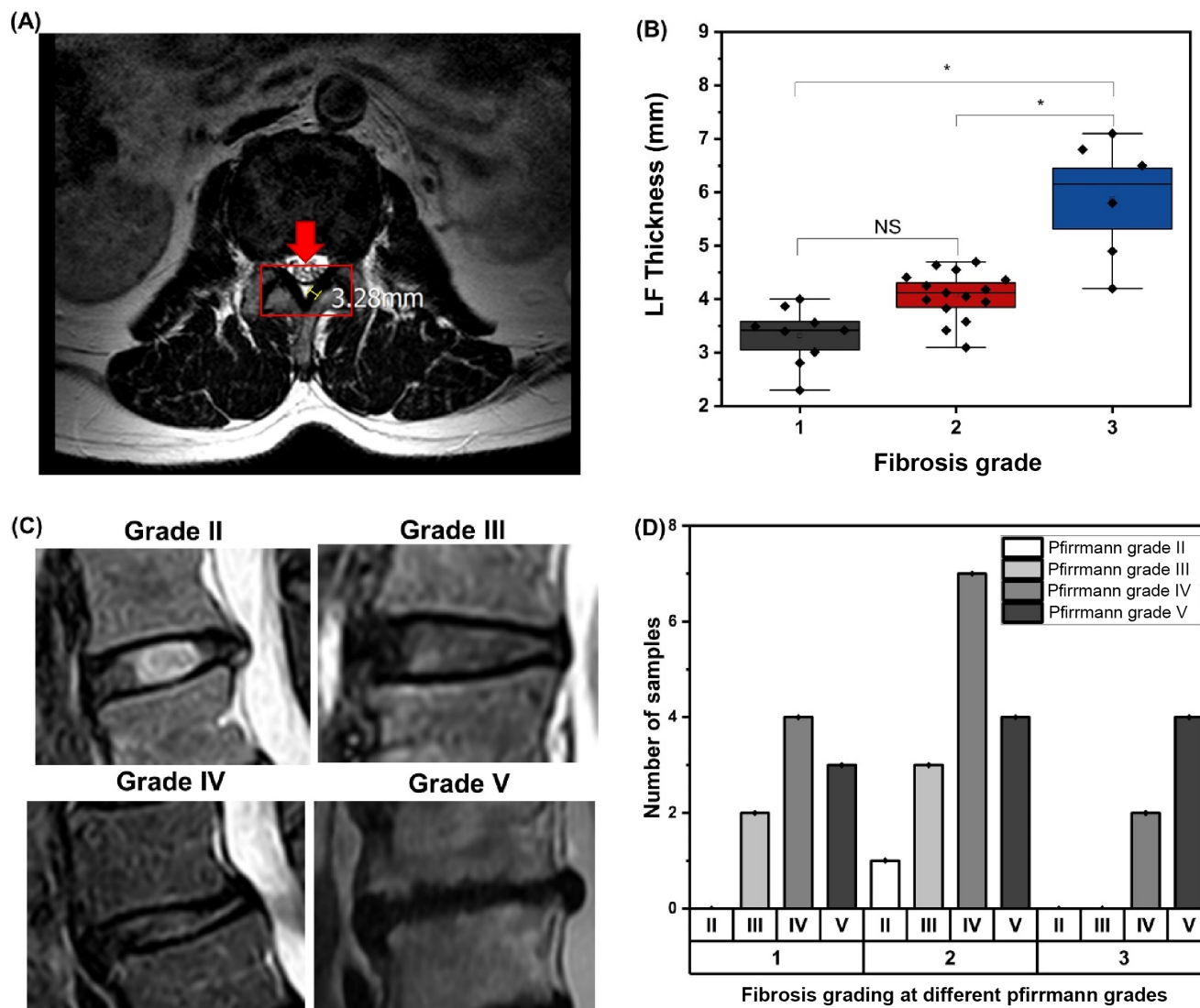
FIGURE 2 (A) Direct visualization of LF thickness within the software interface. The red arrow highlights the LF in its characteristic butterfly shape. (B) Variation in LF thickness across different stages of fibrosis. Higher grades of fibrosis are associated with increased LF thickness. (C) Representative magnetic resonance imaging (MRI) scans of corresponding degenerative disc stages are categorized according to the Pfirrmann classification. Note the absence of Grade I Pfirrmann discs in the analyzed samples. (D) The distribution of fibrosis grades within samples classified by Pfirrmann grades demonstrates that any level of fibrosis can coexist with Pfirrmann grades II to V, suggesting independent progression patterns for these two pathologies. NS, Not statistically different, *: $p < 0.05$.

2 and 3 fibrosis but barely found in grade 1 fibrosis. The peaks corresponding to collagen at ~8, 21.5, and 43° are shown with red line areas. The peaks of collagen at ~8 and ~43° increase in intensity due to degeneration indicate a higher volume fraction of the crystalline phase in the LF.

The minerals peaks appear in grade 2 fibrosis (~19 and 38.5°) and 3 fibrosis (~19, ~28.9, ~38.5, and ~48°). The broad bumps at ~19, 38.5, and ~48° indicate the amorphous structure of calcium phosphate.[23] A sharp peak at ~28.9° could be seen in the spectrum of grade 3 fibrosis of LF sample is well-defined diffraction peaks of hydroxyapatite (HAP).[24] They correspond to a (210) crystal plane with a hexagonal structure. These findings suggest an increase in the

crystallinity of minerals within the LF matrix as degeneration progresses.

3.4 | Molecular components

Raman spectra depicted in Figure 3(B) demonstrate the LF at the different levels of fibrosis. The results presented in this section are proline/hydroxyproline changes (strong peak at 851 cm^{-1}), mineral changes (peak at 958 cm^{-1}), and proteoglycan (1064 and 1370 cm^{-1}) shifts toward the amide I (peak at 1656 cm^{-1}) as the main component of ECM.
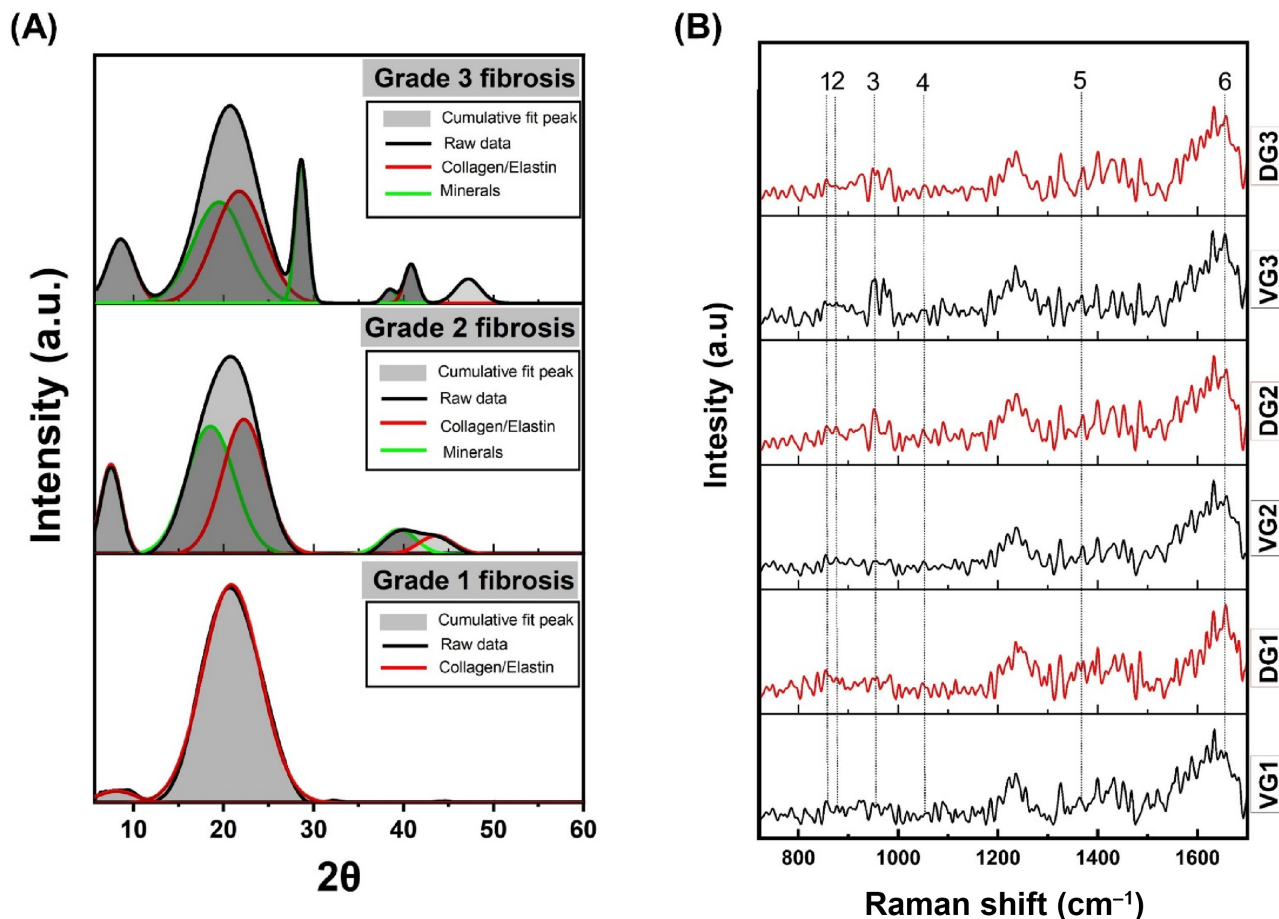
FIGURE 3 Fibrosis progression alters tissue microstructure and biochemical composition. (A) X-ray diffraction (XRD) patterns demonstrate collagen/elastin and mineral presence changes in grade 2 fibrosis, with hydroxyapatite crystals appearing in grade 3 fibrosis. Each graph represents the average of four samples per fibrosis grade (B) Average Raman spectra from all tissue with different grades highlight biochemical shifts across fibrosis grades (VG1-3, DG1-3), including alterations in proline/hydroxyproline (peaks 1 and 2), phosphate (peak 3), proteoglycan groups (peaks 4 and 5), and amide I groups (peak 6) which became the focus of this study. DG, Dorsal Grade; VG, Ventral Grade.

The mineral (phosphate) and proteoglycan characteristics in different fibrosis grades of LF are shown in Figure 4(A,B), respectively. The ratio of phosphate to amide I (I_{958}/I_{1656}) and proteoglycan to amide I ($I_{1064+1370}/I_{1656}$) ratios exhibited statistically significant increases ($p < 0.001$) with advancing fibrosis on both the ventral and dorsal sides of the LF as shown in. This indicates a progressive accumulation of minerals and proteoglycans within the ECM as fibrosis worsens. Notably, the dorsal side consistently displayed slightly higher mineral and proteoglycan content than the ventral side across all fibrosis grades, suggesting potential regional differences in ECM remodeling.

Proline/hydroxyproline, a marker of collagen content, presented a contrasting trend compared to minerals and proteoglycans, as shown in Figure 4(C). The proline/hydroxyproline-to-amide I ratio (I_{851}/I_{1656}) significantly decreased ($p < 0.05$) on the ventral side with increasing fibrosis, indicating a relative reduction in collagen content. However, the $I_{851/1656}$ ratio displayed a less pronounced decline on the dorsal side, showing no statistically significant change ($p = 0.06$). This suggests a potentially slower or less extensive loss of collagen on the dorsal side compared to the ventral side.

3.5 | Biomechanics characteristics

The LF tissue's biomechanical characteristics were elucidated through quasi-static and dynamic measurements. Quasi-static analysis, which assesses the tissue's response under constant load, yielded reduced modulus (Er) and hardness (H). Additionally, dynamic measurements were employed to investigate the tissue's viscoelastic properties. Storage modulus (E′) and loss modulus (E″), obtained through oscillatory testing, quantify the tissue's ability to store and dissipate energy, respectively. The values obtained from these analyses are presented in Figure 5(A–D), offering a comprehensive overview of the LF tissue's mechanical behavior.

Quasi-static measurements revealed a progressive stiffening of the LF tissue with increasing fibrosis grade, as evidenced by the changes in reduced modulus (Er) and hardness (H) shown in Figure 5 (A,B). Er and H demonstrated statistically significant increases ($p < 0.05$) across all fibrosis grades for both ventral and dorsal regions. Notably, there were no statistically significant differences in Er or H within the same fibrosis grade between the ventral and dorsal sides.
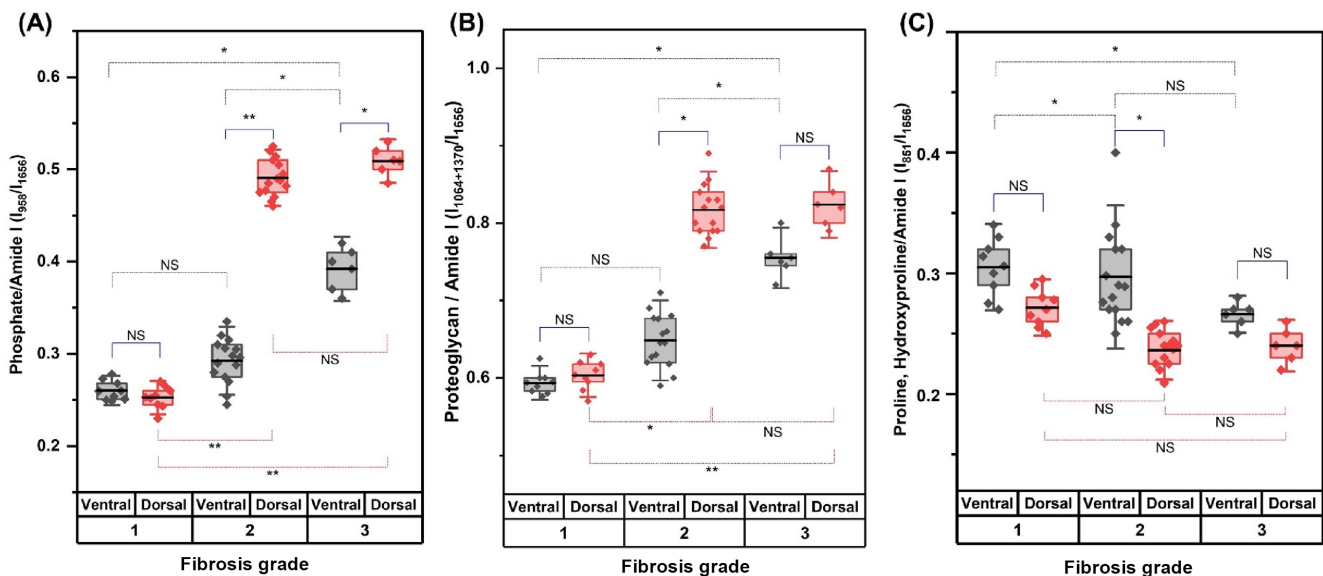
FIGURE 4 Raman markers of fibrosis progression. (A) Phosphate/amide I and (B) Proteoglycan/amide I increase in the ventral and dorsal regions as fibrosis progresses. (C) Proline, Hydroxyproline/amide I show significant changes in the ventral region but remain relatively stable in the dorsal region. NS, Not statistically different. *: $p < 0.05$, **: $p < 0.001$.

However, the dorsal region consistently exhibited slightly higher Er and H values than the ventral region across all fibrosis grades. Specifically, the ventral side Er increased from 4.74 ± 0.40 GPa (grade 1) to 5.41 ± 0.51 GPa (grade 3), while the dorsal side displayed a similar trend, rising from 4.95 ± 0.53 GPa (grade 1) to 5.90 ± 0.53 GPa (grade 3). Similarly, ventral H rose from 0.30 ± 0.03 GPa (grade 1) to 0.33 ± 0.02 GPa (grade 3), while the dorsal H showed a steeper climb from 0.34 ± 0.04 GPa (grade 1) to 0.42 ± 0.02 GPa (grade 3).

Dynamic analysis using NanoDMA further elucidated the viscoelastic behavior of the LF tissue by examining the storage modulus (E′) and loss modulus (E″) as shown in Figure 5(C,D). Both ventral and dorsal E′ exhibited statistically significant increases ($p < 0.05$) with increasing fibrosis grade, indicating stiffer tissue. However, E″ displayed an inverse relationship with fibrosis, demonstrating statistically significant decreases ($p < 0.05$) across all grades for both regions. Ventral E′ rose from 5.09 ± 0.48 GPa (grade 1) to 6.26 ± 0.95 GPa (grade 3), while the dorsal E′ showed a slightly higher increment, increasing from 5.45 ± 0.75 GPa (grade 1) to 6.80 ± 1.09 GPa (grade 3). In contrast, ventral E″ decreased from 0.90 ± 0.14 GPa (grade 1) to 0.63 ± 0.09 GPa (grade 3), with the dorsal region following a similar trend, declining from 0.88 ± 0.17 GPa (grade 1) to 0.63 ± 0.10 GPa (grade 3).

3.6 | Correlation matrix of LF fibrosis variables

The correlation matrix provides a comprehensive overview of the relationships between various factors within the LF, including fibrosis severity, Pfirrmann grading (a measure of disc degenerative changes), LF thickness, and a range of biochemical and biomechanical properties. The correlation matrix reveals several key associations, with LF fibrosis grades as a proxy for fiber alignment and used as the control variable. Detailed results of the correlation analysis can be found in Figure 6, utilizing a color scale ranging from red to black to blue for clarity. The positive and negative correlations are explained as follows:

3.6.1 | Positive correlations

The strong positive correlation ($r_s = 0.74$) between fibrosis grades and LF thickness suggests that as fibrosis progresses, the LF thickens. This finding aligns with the understanding that fibrosis often involves the deposition of excess collagen and other extracellular matrix components, leading to tissue enlargement. as mentioned in the reference [2]. This structural alteration is accompanied by the high positive correlations observed between fibrosis grades and phosphate ($r_s = 0.80$ ventral, $r_s = 0.81$ dorsal) and proteoglycan content ($r_s = 0.87$ ventral, $r_s = 0.73$ dorsal) within the LF, indicating that as fibrosis worsens, these biochemical components accumulate. These biochemical changes, in turn, appear to drive a progressive stiffening of the LF, as evidenced by the positive correlations between fibrosis grades and biomechanical parameters like Er, E′, and H (r_s values ranging from 0.33 to 0.87) which suggest that fibrosis stiffens the LF tissue. While the correlation between fibrosis grades and Pfirrmann grading was not statistically significant ($r_s = 0.21$), the positive trend suggests a potential relationship that warrants further investigation with a larger sample size. The consistent findings across the ventral and dorsal regions of the LF highlight the widespread impact of fibrosis on this tissue.

3.6.2 | Negative correlation

The negative correlations between fibrosis grades and the proline/hydroxyproline ratio ($r_s = -0.49$ ventral, $r_s = -0.55$ dorsal) indicate
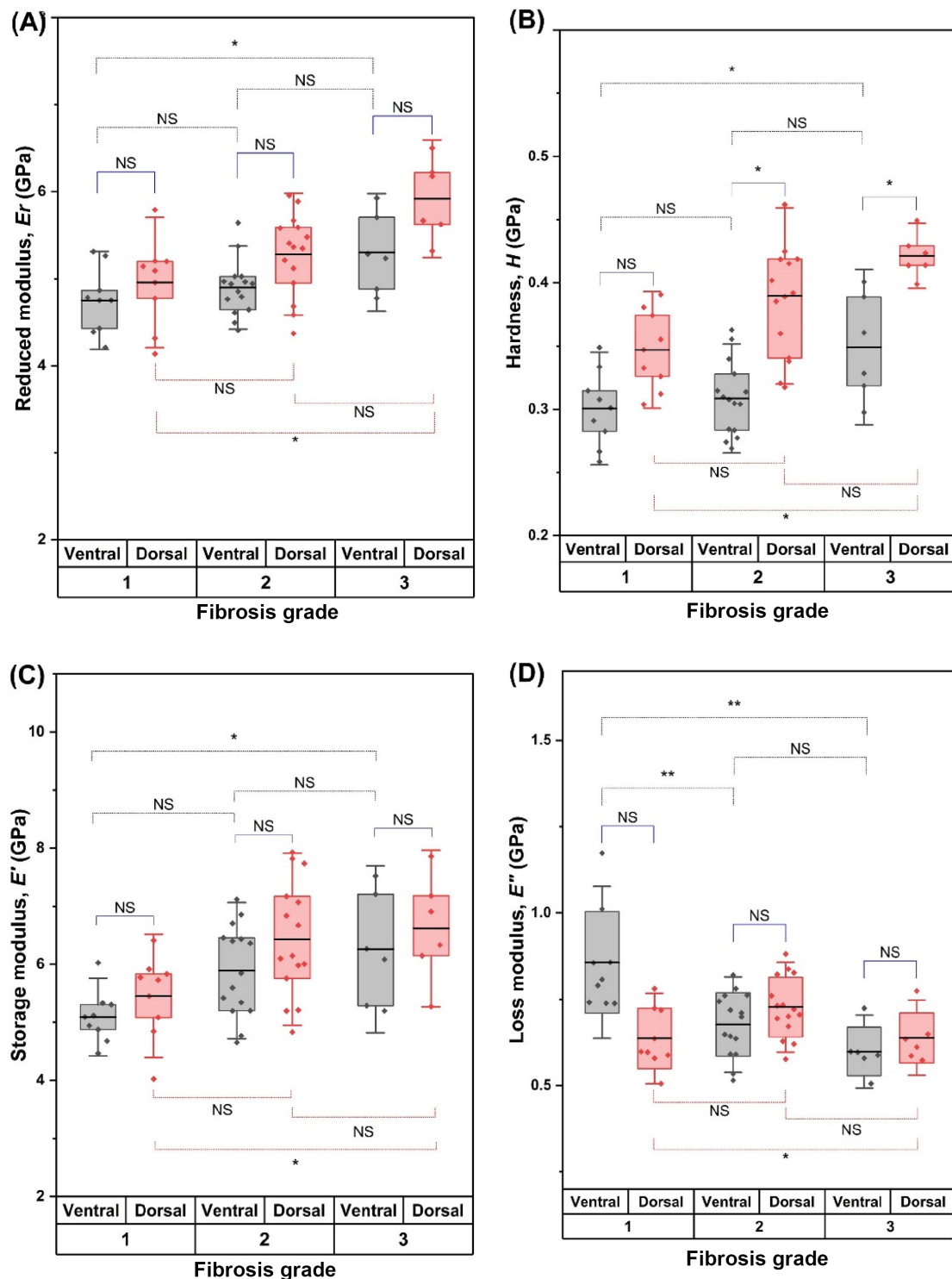
FIGURE 5 Fibrosis grading across fibrosis levels. In all measures (A–D), dorsal values exceed ventral values. (A) Er steadily increases in both regions. (B) H increases sharply in both areas. (C) E′ exhibits a similar increase. (D) E″ shows a decrease in both areas, with the decline more pronounced in the dorsal region. NS, Not statistically different, *: $p < 0.05$, **: $p < 0.001$.

that as fibrosis increases, this ratio decreases. This ratio is often used as an indicator of collagen maturity,[25] and the decrease suggests that fibrosis may be associated with alterations in collagen crosslinking and maturation. Moreover, the negative correlations between fibrosis

grades and the E″ of LF (rs = −0.70 ventral, rs = −0.71 dorsal) imply that as fibrosis progresses, the LF's ability to dissipate energy decreases. This could contribute to the stiffening observed in the positive correlations with other biomechanical parameters.

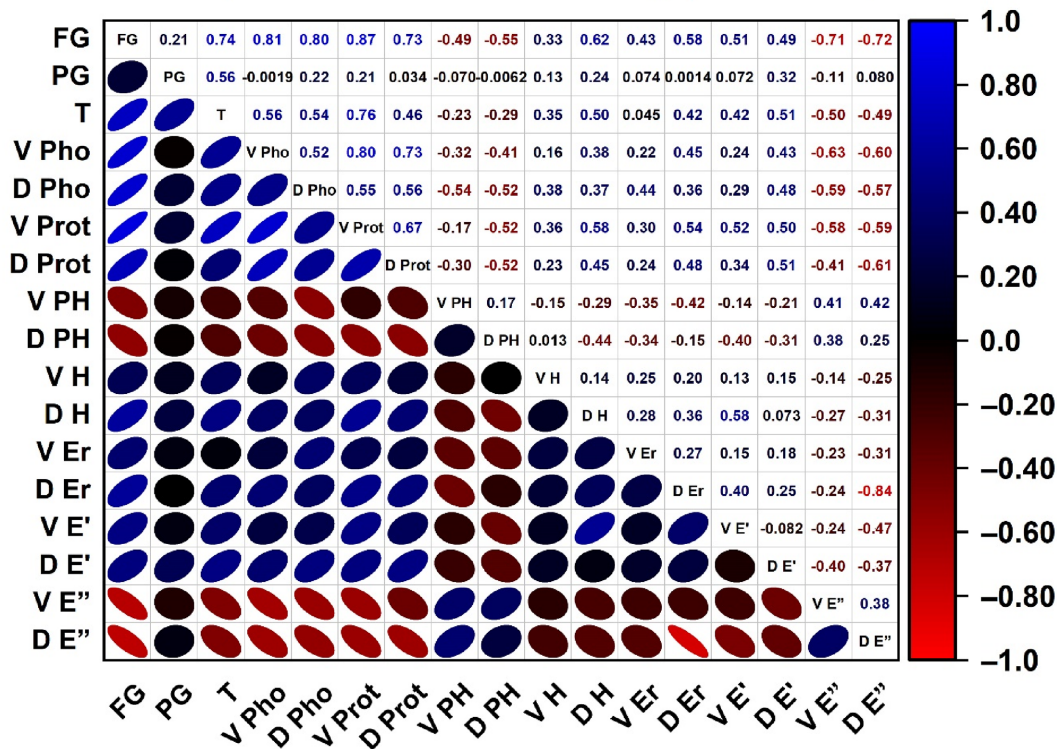## Spearman Correlation (ρ) Heatmap

FIGURE 6 Spearman's rank correlation coefficient (ρ) of LF characteristics across different grades. Lower triangular: Scatter plots with confidence ellipses. Upper triangular: ρ (−1 to +1). Negative values indicate a negative correlation, 0 means no correlation, and positive values indicate a positive correlation. D E″, Dorsal Loss Modulus; D E′, Dorsal Storage Modulus; D Er, Dorsal Reduce Modulus; D H, Dorsal Hardness; D PH, Dorsal Proline/Hydroxyproline; D Pho, Dorsal Phosphate; D Prot, Dorsal Proteoglycan; FG, Fibrosis Grade; PG, Pfirrmann Grade; T, LF Thickness; V E′, Ventral Storage Modulus; V E″, Ventral Loss Modulus; V Er, Ventral Reduced Modulus; V H, Ventral Hardness; V PH, Ventral Proline/Hydroxyproline; V Pho, Ventral Phosphate; V Prot, Ventral Proteoglycan.

4 | DISCUSSION

This study delves deep into the complex landscape of LF degeneration, employing a multi-pronged approach encompassing histological analysis, radiology, microstructure assessment, and spatial biochemical and biomechanical evaluation. By revealing the intricate interplay between various parameters, our findings not only elucidate the multifaceted nature of this pathological process but also pave the way for potential clinical applications, offering hope for the future of LF degeneration treatment.

Our study relies on histological staining as the cornerstone for fibrosis classification, providing a clear visual of the transformation as degeneration advances. The once-ordered structure of elastic fibers gives way to disarray, and hyalinized collagen gradually replaces a significant portion of their presence. This mirrors the established wound healing mechanisms involving elastic fiber loss and heightened collagen deposition.[26] Radiological evaluation echoed these observations, demonstrating a clear correlation between increased fibrosis grades and LF thickening. Notably, this thickening displayed dependence on the intervertebral disc (IVD) degeneration level, as reflected by the Pfirrmann classification, highlighting the intricate interdependence between LF and IVD in maintaining spinal integrity and function.

Our study utilizes XRD analysis to delve into the atomic underpinnings of LF degeneration. This advanced technique reveals a significant shift in the collagen signature within healthy LF tissue as degeneration progresses. The intensity of characteristic collagen peaks at 8 and 43° increases with higher fibrosis grades, indicating a growing volume fraction of the crystalline phase and a heightened organization of tightly packed collagen fibers. The emergence of mineral peaks in grades 2 and 3 fibrosis further suggests altered mineralization patterns alongside collagen reorganization.

Notably, the soft tissue's amorphous components, comprised mainly of proteins and collagen fibers, play a crucial role in its functionality and mechanical behavior, evidently viscoelasticity.[27] Therefore, the observed transition from amorphous to crystalline microstructure is a potent indicator of the underlying pathological processes within the degenerated LF tissue. In essence, XRD analysis provides compelling evidence that increasing degeneration in the LF translates to significant changes at the atomic level, shedding light on the tissue's altered biomechanical properties and potentially paving the way for novel therapeutic strategies targeting these structural transformations.

Raman spectroscopy, a powerful analytical tool, unveils the biochemical hallmarks of LF degeneration at the molecular level.

This study focuses on three critical biomarkers: mineralization, proteoglycan, and proline/hydroxyproline, offering more profound insights into the pathological processes at different fibrosis stages.

Mineralization: The ratio of phosphate to amide I, captured by Raman spectroscopy, is a sensitive indicator of mineral deposits within the LF tissue. Our findings reveal a direct correlation between the severity of LF fibrosis and the concentration of these mineral deposits. This increased mineralization, often associated with soft tissue damage and aging [41], could be further exacerbated by trauma-induced tissue stiffening and impaired nutrient absorption.[28] Interestingly, the spatial analysis demonstrates a more pronounced increase in mineral deposits on the dorsal side of the LF compared to the ventral side. This suggests that the dorsal region might be more susceptible to injury and subsequent degenerative changes.

Proteoglycans: These complex molecules, rich in glycosaminoglycan and biglycan chains, play a crucial role in cellular signaling pathways,[29] regulating processes like growth, proliferation, adhesion, and wound healing. In pathological states, however, proteoglycans contribute to tissue repair through mechanisms involving inflammation, fibrosis, and collagen deposition.[30] Our data aligns with this notion, showing elevated proteoglycan levels in the LF ECM as fibrosis worsens, particularly in grade 3, where focal hyalinized collagen deposits are observed. This suggests mechanical stress and injury drive tissue remodeling and collagen deposition during severe degeneration, triggering proteoglycan activity. Our findings on proteoglycan changes content in the LF, as detected by Raman spectroscopy, offer valuable insights that both align with and expand upon previous research. Notably, our work complements Salimi's findings. et al. highlighted the role of biglycan (a specific proteoglycan) in expression in hypertrophied LF and explored the role of proteoglycan accumulation in LF cells.[31] Similarly, our observations regarding proteoglycans resonate with the work of Yabe et al., who reported increased proteoglycans in patients with lumbar spinal canal stenosis.[32] Moreover, Yukawa et al. focus on structural varieties of small proteoglycans in the LF, which provides a foundation for interpreting spectral variations detected in our study.[33] Integrating our Raman-based methodology with these previous studies offers a more comprehensive perspective on the complex biochemical alterations within the degenerating LF. Further investigations combining Raman spectroscopy with targeted analysis of specific proteoglycans or their molecular constituents could yield an even deeper understanding of LF pathology, potentially leading to the identification of novel biomarkers or therapeutic targets for spinal conditions.

Proline/hydroxyproline: This amino acid plays a vital role in stabilizing the collagen triple helix, and its structural alterations can lead to protein denaturation.[34] While our study reveals subtle changes in the proline/hydroxyproline-to-amide I ratio, mainly a slight decrease on the ventral side in grade 2 fibrosis, further investigation is needed to understand its role in the fibrotic process fully.

Based on the observed confidence levels, phosphate is the most reliable biomarker for assessing LF fibrosis severity, followed by proteoglycan and proline/hydroxyproline. This ranking underscores the importance of focusing on mineralization and proteoglycan activity when evaluating the extent of degenerative changes in the LF tissue. The Raman analysis paves the way for further exploration of the intricate molecular mechanisms governing LF degeneration. From the specific finding, elucidating the precise role of proline/hydroxyproline and delving deeper into the spatial variations in biochemical composition could hold significant potential for developing targeted therapeutic interventions for this debilitating condition.

This paragraph delves into the biomechanical consequences of LF degeneration, revealing how changes in tissue composition translate into altered mechanical properties. Using NanoDMA, a sophisticated tool for analyzing microscopic material behavior, we investigated the quasi-static and dynamic properties of LF samples across various fibrosis grades.

Increasing rigidity: Our findings clearly show that as fibrosis worsens, the LF exhibits a marked increase in reduced modulus and hardness. This translates to stiffer and less compliant tissue, a direct consequence of the progressive replacement of elastic fibers with collagen during degeneration. Interestingly, the dorsal side of the LF demonstrates a more pronounced stiffening effect compared to the ventral side, suggesting a differential susceptibility to mechanical stress and potentially explaining the discordant degeneration patterns observed in some cases.

Viscoelastic nature: Dynamic analysis provides valuable insights into the viscoelastic nature of LF tissue. The observed dominance of the storage modulus over the loss modulus signifies that, at the microscopic level, the LF behaves predominantly as an elastic material. However, with increasing fibrosis severity, the storage modulus rises while the loss modulus falls. This implies a further stiffening of the tissue and a decline in its ability to dissipate energy and absorb stress, vital functions for maintaining spinal stability during movement.

Elasticity compromised: The crucial role of elastic fibers in LF function cannot be overstated. As the primary extracellular matrix component in healthy LF, these fibers contribute significantly to the tissue's extensibility and shock absorption capacity through their inherent viscoelastic properties. The progressive substitution of elastic fibers with collagen disrupts this delicate balance, compromising the LF's ability to adapt to mechanical demands and potentially contributing to spinal instability.

Biomechanical markers: Our study highlights the potential of biomechanical characteristics as valuable markers for monitoring LF degeneration progression. The observed changes in stiffness, particularly the disparity between the dorsal and ventral sides, provide additional diagnostic tools and may offer insights into the underlying biomechanical mechanisms driving this complex pathological process.

Further research is warranted to investigate the intricate relationship between LF composition, structure, and biomechanical behavior. Understanding the regional variations in mechanical properties and their relation to the finite element modeling data[26] could pave the way for developing personalized treatment strategies and optimizing spinal interventions for patients with LF degeneration.

Clinical relevance of this study is: (1) *Targeted Treatment*: The knowledge that most mechanical and biochemical characteristics alterations in the dorsal side of the LF are more prominent than in the ventral part due to degeneration can help clinicians develop targeted interventions to address the specific mechanical changes associated with LF degeneration. For example, treatment modalities that focus on reducing stiffness and improving flexibility in a particular area of LF may be considered.

Moreover, it can enhance the establishment of new approaches for LFH treatments, such as decorin therapy[5] and Oxidative Stress therapy.[6] Another possible treatment is to recover the viscoelastic properties and prevent the degeneration of the LF by inhibiting total collagen production, such as the treatment with COX-2 inhibitors.[35] (2) *Surgical Planning*: Knowledge of crystalline minerals' spatial characteristics and presence in severely degenerated LF can help surgeons plan surgical procedures. They can focus on addressing the specific areas of degeneration and stiffness during the surgical intervention, potentially leading to better outcomes. (3) *Customized Rehabilitation*: Understanding the spatial mechanical characteristics of the LF can also inform the design of rehabilitation programs. Rehabilitation specialists can tailor exercises and therapies to target specific areas of stiffness and degeneration. This personalized approach may enhance the effectiveness of rehabilitation in improving flexibility, reducing pain, and restoring function. (4) *Preventive Measures*: The early and severe stages of fibrosis can occur in any level of degenerative lumbar discs based on MRI assessment of the Pfirrman grades. LF degeneration is intercorrelated with disc degeneration; hence, the early assessment, such as the Oswestry Disability Index (ODI) and the Visual Analog Scale (VAS), may correlate with this study's key finding.

Several limitations need consideration. This study focused on the biomechanical and biomolecular changes associated with fibrosis in the LF. However, it is essential to consider that chondrogenesis, transforming tissue into cartilage-like structures, can also significantly contribute to LF degeneration. Several studies have demonstrated the presence of chondroid metaplasia in degenerated LF tissue[36] and increasing expression of bone morphogenetic protein (BMP).[37] Future studies could combine our methods with complementary techniques like histological staining or gene expression analysis to better understand LF degeneration. This would illuminate the interplay between fibrosis and chondrogenesis within the LF.

Additionally, expanding the scope of future studies to include samples representing a broader range of degenerative states, along with an updated scoring system involving various parameters, could help elucidate the relative contributions of these processes at different stages of LF pathology. Moreover, a lack of a control group impedes direct comparison with healthy tissues. Clinical relevance might be improved by assessing the impact of LF degeneration on patient symptoms and outcomes. Future research could involve larger patient cohorts, incorporating control groups and longitudinal assessments.

5 | CONCLUSION

The multidimensional approach of this study provides a comprehensive understanding by linking microstructure with XRD, spatial biochemistry with Raman spectroscopy, spatial biomechanics with instrumented nanoindentation, and radiological features in MRI of LF degeneration. This approach holds significant clinical implications as it enhances diagnostic accuracy and provides a comprehensive pathological characterization. Therefore, it may be beneficial for facilitating personalized treatment approaches, enabling treatment monitoring and outcome evaluation to provide prompt treatment to delay the

process of degeneration and save the patient from developing long-term morbidity. Additionally, this evaluation method can drive advancements in research and technology for the better management of LF degeneration and contribute to advancements in tissue engineering related to tissue degeneration.

AUTHOR CONTRIBUTIONS

A.A. and K.Y.H. writing – original draft and review & editing; A.A., K.Y.H., H.Y.L., W.L.L., and W.A.L. performed methodology; A.A., J.H., and W.A.L. investigation and validation; Y.R.J. funding acquisition, conceptualization, supervision, and writing – review & editing. All authors read and approved the final paper.

CONFLICT OF INTEREST STATEMENT

The author(s) have no conflicts of interest relevant to this article.

ORCID

Azril Azril https://orcid.org/0000-0001-8685-5517
Kuo-Yuan Huang https://orcid.org/0000-0003-2153-5664
Wen-Lung Liu https://orcid.org/0000-0002-5062-7106
Yeau-Ren Jeng https://orcid.org/0000-0001-6787-1538

REFERENCES

1. Okuda T, Fujimoto Y, Tanaka N, Ishida O, Baba I, Ochi M. Morphological changes of the ligamentum flavum as a cause of nerve root compression. *Eur Spine J*. 2005;14(3):277-286. doi:10.1007/s00586-004-0782-5
2. Okuda T, Baba I, Fujimoto Y, et al. The pathology of ligamentum flavum in degenerative lumbar disease. *Spine (Phila Pa 1976)*. 2004; 29(15):1689-1697. doi:10.1097/01.BRS.0000132510.25378.8C
3. Daffner SD, Wang JC. The pathophysiology and nonsurgical treatment of lumbar spinal stenosis. *Instr Course Lect*. 2009;58:657-668.

4. Beamer YB. Hypertrophied ligamentum flavum. *Arch Surg*. 1973; 106(3):289. doi:10.1001/archsurg.1973.01350150029008

5. Wang S, Qu Y, Fang X, et al. Decorin: a potential therapeutic candidate for ligamentum flavum hypertrophy by antagonizing TGF-β1. *Exp Mol Med*. 2023;55:1413-1423. doi:10.1038/s12276-023-01023-y

6. Ito K, Kise H, Suzuki S, et al. Potential involvement of oxidative stress in ligamentum flavum hypertrophy. *J Clin Med*. 2023;12(3):808. doi:10.3390/jcm12030808

7. Miyasaka K, Kaneda K, Sato S, et al. Myelopathy due to ossification or calcification of the ligamentum flavum: radiologic and histologic evaluations. *Am J Neuroradiol*. 1983;4(3):629-632.

8. Beyhaghi M, Hobley J, Rouhani M, Jeng Y-R. Quasi-honeycomb grain morphologies strengthen passivating layers in Inconel-718 superalloy: lessons learned from additive manufacturing. *Appl Surf Sci*. 2023;612: 155735. doi:10.1016/j.apsusc.2022.155735

9. Beyhaghi M, Rouhani M, Hobley J, Jeng Y-R. In-situ and ex-situ comparison of oxidation of Inconel 718 manufactured by selective laser melting and conventional methods up to 650°C. *Appl Surf Sci*. 2021; 569:151037. doi:10.1016/j.apsusc.2021.151037

10. Rouhani M, Hobley J, Ou HH, Lee JT, Metla SBS, Jeng YR. A new gateway to ecofriendly self-healing amorphous carbon tribofilms from ancient oils. *Appl Mater Today*. 2022;29:101616. doi:10.1016/j.apmt.2022.101616

11. Jeng YR, Tan CM. Study of nanoindentation using FEM atomic model. *J Tribol*. 2004;126(4):767-774. doi:10.1115/1.1792679

12. Jywe W-Y, Jeng YR, Liu CH, et al. A novel 5DOF thin coplanar nanometer-scale stage. *Precis Eng*. 2008;32(4):239-250. doi:10.1016/j.precisioneng.2007.11.001

13. Miyamori D, Uemura T, Zhu W, et al. A Raman algorithm to estimate human age from protein structural variations in autopsy skin samples: a protein biological clock. *Sci Rep*. 2021;11(1):1-8. doi:10.1038/s41598-021-85371-7

14. Azril K, Huang J, Hobley M, Rouhani WL, Jeng Y. Correlation of the degenerative stage of a disc with magnetic resonance imaging, chemical content, and biomechanical properties of the nucleus pulposus. *J Biomed Mater Res A*. 2022;111:1054-1066. doi:10.1002/jbm.a.37490

15. Smith E, Dent G. *Modern Raman Spectroscopy - A Practical Approach*. John Wiley and Sons; 2005. doi:10.1002/0470011831

16. Azril, Huang K-Y, Hobley M, Rouhani WL, Liu W-L, Jeng Y-R. A methodology to evaluate different histological preparations of soft tissues: intervertebral disc tissues study. *J Appl Biomater Funct Mater*. 2023; 21:228080002311556. doi:10.1177/22808000231155634

17. Pfirrmann CWA, Metzdorf A, Zanetti M, Hodler J, Boos N. Magnetic resonance classification of lumbar intervertebral disc degeneration. *Spine (Phila Pa 1976)*. 2001;26(17):1873-1878. doi:10.1097/00007632-200109010-00011

18. Rouhani M, Hobley J, Hong FCN, Jeng YR. Spectroscopic investigation of thermally induced structural evolution of a-C:H:Si film. *Appl Surf Sci*. 2021;541:148413. doi:10.1016/j.apsusc.2020.148413

19. Khalid M, Bora T, Al Ghaithi A, Thukral S, Dutta J. Raman spectroscopy detects changes in bone mineral quality and collagen crosslinkage in staphylococcus infected human bone. *Sci Rep*. 2018;8(1):1-9. doi:10.1038/s41598-018-27752-z

20. Cohen J. *Statistical Power Analysis for the Behavioral Sciences*. 2nd ed. Lawrence Erlbaum Associates, Publishers; 1998.

21. Sun TW, Zhu YJ, Chen F. Hydroxyapatite nanowire/collagen elastic porous nanocomposite and its enhanced performance in bone defect repair. *RSC Adv*. 2018;8(46):26218-26229. doi:10.1039/c8ra03972k

22. Xu Z, Guan X, Liu J, Fan H, Chen Y. Improving collagen extraction through an alternative strategy based on succinic anhydride pretreatment to retain collagen's triple-helix structure. *J Appl Polym Sci*. 2017; 134(42):45424. doi:10.1002/app.45424

23. Dorozhkin SV. Synthetic amorphous calcium phosphates (ACPs): preparation, structure, properties, and biomedical applications. *Royal Soc Chem*. 2021;9:7748. doi:10.1039/d1bm01239h

24. Iafisco M, Foltran I, Sabbatini S, Tosi G, Roveri N. Electrospun nanostructured fibers of collagen-biomimetic apatite on titanium alloy. *Bioinorg Chem Appl*. 2012;2012:1-8. doi:10.1155/2012/123953

25. Albaugh VL, Mukherjee K, Barbul A. Proline precursors and collagen synthesis: biochemical challenges of nutrient supplementation and wound healing. *J Nutr*. 2017;147(11):2011-2017. doi:10.3945/jn.117.256404

26. Sairyo K, Biyani A, Goel V, et al. Pathomechanism of ligamentum flavum hypertrophy: a multidisciplinary investigation based on clinical, biomechanical, histologic, and biologic assessments. *Spine (Phila Pa 1976)*. 2005;30:2649-2656. Available: http://journals.lww.com/spinejournal

27. Kirkness MW, Lehmann K, Forde NR. Mechanics and structural stability of the collagen triple helix. *Curr Opin Chem Biol*. 2019;53:98-105. doi:10.1016/j.cbpa.2019.08.001

28. Banks KP, Bui-Mansfield LT, Chew FS, Collinson F. A compartmental approach to the radiographic evaluation of soft-tissue calcifications. *Semin Roentgenol*. 2005;40(4):391-407. doi:10.1053/j.ro.2005.01.021

29. Puri S, Coulson-Thomas YM, Gesteira TF, Coulson-Thomas VJ. Distribution and function of glycosaminoglycans and proteoglycans in the development, homeostasis and pathology of the ocular surface. *Front Cell Dev Biol*. 2020;8:731. doi:10.3389/fcell.2020.00731

30. Ghatak S, Maytin EV, Mack JA, et al. Roles of proteoglycans and glycosaminoglycans in wound healing and fibrosis. *Int J Cell Biol*. 2015; 2015:834893. doi:10.1155/2015/834893

31. Salimi H, Suzuki A, Habibi H, et al. Biglycan expression and its function in human ligamentum flavum. *Sci Rep*. 2021;11(1):4867. doi:10.1038/s41598-021-84363-x

32. Yabe Y, Hagiwara Y, Tsuchiya M, et al. Decreased elastic fibers and increased proteoglycans in the ligamentum flavum of patients with lumbar spinal canal stenosis. *J Orthop Res*. 2016;34(7):1241-1247. doi:10.1002/jor.23130

33. Yukawa M, Takagaki K, Itabashi T, Ueyama K, Harata S, Endo M. Structural varieties of small proteoglycans in human spinal ligament. *Connect Tissue Res*. 2001;42(3):209-222. doi:10.3109/03008200109005651

34. Fischer Verlag G, Brodsky B, Ramshaw JAM. The collagen triple-helix structure. *Matrix Biol*. 1997;15:545-554.

35. Esbona K, Inman D, Saha S, et al. COX-2 modulates mammary tumor progression in response to collagen density. *Breast Cancer Res*. 2016; 18(1):35. doi:10.1186/s13058-016-0695-3

36. Yabe Y, Hagiwara Y, Ando A, et al. Chondrogenic and fibrotic process in the ligamentum flavum of patients with lumbar spinal canal stenosis. *Spine (Phila Pa 1976)*. 2015;40(7):429-435. doi:10.1097/BRS.0000000000000795

37. Shafaq N, Suzuki A, Terai H, Wakitani S, Nakamura H. Cellularity and cartilage matrix increased in hypertrophied ligamentum flavum. *J Spinal Disord Tech*. 2012;25(2):107-115. doi:10.1097/BSD.0b013e31820bb76e

SUPPORTING INFORMATION

Additional supporting information can be found online in the Supporting Information section at the end of this article.